

## ARTICLES

# Structure of a $\beta_1$ -adrenergic G-protein-coupled receptor

Tony Warne<sup>1</sup>, Maria J. Serrano-Vega<sup>1</sup>, Jillian G. Baker<sup>2</sup>, Rouslan Moukhametzianov<sup>1</sup>, Patricia C. Edwards<sup>1</sup>, Richard Henderson<sup>1</sup>, Andrew G. W. Leslie<sup>1</sup>, Christopher G. Tate<sup>1</sup> & Gebhard F. X. Schertler<sup>1</sup>

**G-protein-coupled receptors have a major role in transmembrane signalling in most eukaryotes and many are important drug targets. Here we report the 2.7 Å resolution crystal structure of a  $\beta_1$ -adrenergic receptor in complex with the high-affinity antagonist cyanopindolol. The modified turkey (*Meleagris gallopavo*) receptor was selected to be in its antagonist conformation and its thermostability improved by earlier limited mutagenesis. The ligand-binding pocket comprises 15 side chains from amino acid residues in 4 transmembrane  $\alpha$ -helices and extracellular loop 2. This loop defines the entrance of the ligand-binding pocket and is stabilized by two disulphide bonds and a sodium ion. Binding of cyanopindolol to the  $\beta_1$ -adrenergic receptor and binding of carazolol to the  $\beta_2$ -adrenergic receptor involve similar interactions. A short well-defined helix in cytoplasmic loop 2, not observed in either rhodopsin or the  $\beta_2$ -adrenergic receptor, directly interacts by means of a tyrosine with the highly conserved DRY motif at the end of helix 3 that is essential for receptor activation.**

G-protein-coupled receptors (GPCRs) are a large family of integral membrane proteins that are prevalent in eukaryotes from yeast to man, and function as key intermediaries in the transduction of signals from outside to inside the cell<sup>1</sup>. Activating molecules (agonists), such as hormones and neurotransmitters, bind to GPCRs from the extracellular side of the cell membrane and induce a large conformational change that propagates to the cytoplasmic surface<sup>2,3</sup>, resulting in activation of G proteins and a consequent change in the level of intracellular messengers such as cAMP, Ca<sup>2+</sup> or signalling lipids. There are over 800 different human GPCRs<sup>4</sup>, all of which share the characteristic arrangement of 7 transmembrane  $\alpha$ -helices, with the polypeptide amino terminus on the extracellular side of the plasma membrane<sup>5</sup>.

Analysis of the primary amino acid sequences of GPCRs has resulted in the definition of a number of families<sup>6</sup>, the largest of which, family A, includes the archetypal GPCR, rhodopsin. The three human  $\beta$ -adrenergic receptor ( $\beta$ AR) subtypes,  $\beta_1$ ,  $\beta_2$  and  $\beta_3$ , belong to family A and share 51% sequence identity between Trp<sup>1.31</sup>–Asp<sup>5.73</sup> and Glu<sup>6.30</sup>–Cys<sup>H8-Cterm</sup>; that is, excluding the amino and carboxy termini and most of cytoplasmic loop 3 (Supplementary Fig. 1; superscripts refer to Ballesteros–Weinstein numbering<sup>7</sup>). Drugs that inhibit  $\beta_1$  and  $\beta_2$  receptor signalling (antagonists and inverse agonists) are used to modulate heart function and are known as  $\beta$ -blockers<sup>8</sup>, but selective  $\beta_1$ -antagonists are preferred because they have fewer side effects due to bronchial constriction by means of  $\beta_2$  receptors in the lung. In contrast to the  $\beta_1$  and  $\beta_2$  receptors, the  $\beta_3$ -adrenergic receptor ( $\beta_3$ AR) is found in adipose tissue, where adrenaline stimulates metabolism, and is a potential target to treat obesity. Elucidation of the specificity determinants for drug affinity of the different  $\beta$ AR subtypes will allow the development of better subtype-specific  $\beta$ -blockers, with fewer side effects.

A milestone in the study of  $\beta$ ARs was recently reached with the publication of a  $\beta_2$ -adrenergic receptor ( $\beta_2$ AR) structure in a complex with an antibody fragment,  $\beta_2$ AR–Fab<sup>9</sup>, followed by the higher resolution structure of an engineered  $\beta_2$ AR fused in the middle of the third cytoplasmic loop (CL3) to T4 lysozyme,  $\beta_2$ AR–T4 (ref. 10).

These structures, both containing the high affinity antagonist carazolol, defined the overall architecture of  $\beta_2$ AR and the structure of the ligand-binding pocket. However, the structures also raised questions of how a range of compounds can bind to the different but closely related  $\beta$ AR subtypes with different affinities. For example, the human  $\beta_1$  and  $\beta_2$  receptors are 67% identical within their transmembrane regions, but the residues that directly surround the ligand-binding pocket appear to be identical. Despite these similarities, larger antagonists such as CGP 20712A (see Supplementary Fig. 2) bind 500 times more strongly to  $\beta_1$ AR than to  $\beta_2$ AR, whereas ICI 118551 shows a 550-fold specificity for  $\beta_2$ AR over  $\beta_1$ AR<sup>11</sup>. There are also  $\beta_1$ - and  $\beta_2$ -specific agonists<sup>12</sup>. As an important step towards understanding subtype specificity, we have determined the structure of a  $\beta_1$ -adrenergic receptor ( $\beta_1$ AR).

## Crystallization of $\beta_1$ AR

GPCR crystallization is challenging, because GPCRs are usually unstable in detergent, contain unstructured regions and spontaneously cycle between an inactive antagonist state (*R*) and an active agonist state (*R\**), which may further decrease the stability<sup>13</sup>. The human  $\beta_1$ AR is more difficult to purify than  $\beta_2$ AR because it is very unstable in detergent. We therefore used turkey (*M. gallopavo*)  $\beta_1$ AR, which is more stable than human  $\beta_1$ AR<sup>14</sup> although less stable than human  $\beta_2$ AR (M.J.S.-V. and C.G.T., unpublished observation). A mutated receptor,  $\beta_1$ AR–m23, was constructed with enhanced thermostability over the wild-type receptor and an altered equilibrium between *R* and *R\** so that the mutant receptor was preferentially in the antagonist (*R*) state<sup>15</sup>. The receptor construct,  $\beta_1$ AR36–m23 (Fig. 1), purified in octylthioglucoside and in the presence of cyanopindolol gave good crystals showing isotropic diffraction beyond 2.7 Å.

## Pharmacological analysis of $\beta_1$ AR–m23

The mutant receptor  $\beta_1$ AR–m23 bound the antagonists dihydroalprenolol and cyanopindolol with similar affinities to the wild-type receptor, but the agonists noradrenaline and isoprenaline bound

<sup>1</sup>MRC Laboratory of Molecular Biology, Hills Road, Cambridge CB2 0QH, UK. <sup>2</sup>Institute of Cell Signalling, Medical School, Queen's Medical Centre, University of Nottingham, Nottingham NG7 2UH, UK.

more weakly by a factor of 2,470 and 650, respectively<sup>15</sup>. This reflects a change in the  $R$  to  $R^*$  equilibrium of the receptor towards the antagonist  $R$  state. From this we predicted that, in a G-protein-coupling assay, the receptor would show no basal activity and that the concentration of agonist required for signalling would be orders of magnitude higher. Signalling assays were performed on stable cell lines expressing the wild-type  $\beta_1$ AR truncated at the N and C termini ( $\beta_1$ ARtrunc) and also containing the six thermostabilizing mutations (m23) (Supplementary Fig. 3).  $\beta_1$ ARtrunc-m23 coupled efficiently to G proteins and elicited a robust stimulation of cAMP-responsive reporter gene, although the agonist concentration response curve, as expected, was shifted to the right<sup>16</sup>. The drug ICI 118551, an inverse agonist for both  $\beta_1$ AR<sup>17</sup> and  $\beta_2$ AR<sup>18</sup>, showed no reduction in the basal level of cAMP when added at a concentration 100-fold above its inhibition constant ( $K_i$ ) to cells containing  $\beta_1$ ARtrunc-m23, implying there is negligible basal constitutive activity. The structure we have determined contains the very high affinity antagonist cyanopindolol in the binding pocket and represents closely the inactive conformation with respect to G-protein coupling.

### Overall structure and the extracellular loops

The structure was solved by molecular replacement to 2.7 Å resolution with an  $R_{\text{work}}$  of 0.212 and an  $R_{\text{free}}$  of 0.268 (Supplementary Table 1). The four receptor molecules in the unit cell, labelled A–D (Supplementary Figs 4–6), were all very similar except that molecules A and D both had a 60° kink in helix 1 (H1). Also modelled were 31 water molecules, 4 Na<sup>+</sup> ions and 14 detergent molecules (see Supplementary Information). Unless otherwise stated, all further discussion refers to molecule B, because this molecule has an unkinked H1 and a relatively well-ordered H8. The helix boundaries, disordered regions and overall structural motifs are presented in Fig. 1.

The amino acid sequence of turkey  $\beta_1$ AR<sup>19</sup> is 82% and 67% identical to human  $\beta_1$ AR and human  $\beta_2$ AR, respectively, over residues Trp40<sup>1.31</sup>–Asp242<sup>5.73</sup> and Glu285<sup>6.30</sup>–Cys358<sup>H8-Cterm</sup> (that is, excluding the N and C termini and most of CL3); it is therefore expected that the structure of the transmembrane regions of  $\beta_1$ AR

and  $\beta_2$ AR should be very similar. Our superposition of  $\beta_2$ AR (Protein Data Bank, PDB, code 2RH1) and  $\beta_1$ AR (chain B) is based on selected residues in H3, H5, H6 and H7 because we were particularly interested in comparing the ligand-binding pockets; 78 C $\alpha$  atoms can be superimposed with a root mean square deviation (r.m.s.d.) of 0.25 Å. The r.m.s.d. over all transmembrane helices is 0.7 Å (269 C $\alpha$  atoms; Supplementary Fig. 7). Comparison of the structures of  $\beta_1$ AR and  $\beta_2$ AR reveals no evidence for any significant changes in backbone conformation at the sites of the six point mutants introduced<sup>15</sup> to stabilize  $\beta_1$ AR. This is consistent with the observation that  $\beta_1$ AR-m23 binds antagonists with similar affinities to the wild-type receptor<sup>15</sup> and that it can couple efficiently to G proteins, although at higher agonist concentration (Supplementary Fig. 3). The basis for the thermostabilization by the six mutations R68<sup>1.59</sup>S, M90<sup>2.53</sup>V, Y227<sup>5.58</sup>A, A282<sup>6.27</sup>L, F327<sup>7.37</sup>A and F338<sup>7.48</sup>M is not immediately apparent from the structure.

The structures of the three extracellular loops (EL1–3) in  $\beta_1$ AR are very similar to those of  $\beta_2$ AR (C $\alpha$  r.m.s.d. of 0.8 Å), consistent with the high sequence conservation of these regions in the  $\beta$ AR family (Supplementary Fig. 1). On the extracellular surface, a clear peak in the electron density is present at a position co-ordinated by the backbone carbonyl groups of residues Cys 192, Asp 195, Cys 198 and one or two water molecules (Supplementary Fig. 8). This density was assigned to a sodium ion on the basis of its coordination geometry<sup>20</sup>. Its role, bound at the negative end of the EL2  $\alpha$ -helix dipole, may be to stabilize the helical conformation of EL2 and thus the structure of the entrance to the ligand-binding pocket. The large difference in EL2 conformation between the  $\alpha$ -helix found in  $\beta_2$ AR and the  $\beta$ -hairpin that closes off the retinal-binding site in rhodopsin is confirmed in the structure of  $\beta_1$ AR, suggesting that the  $\alpha$ -helix may be a common feature in those GPCRs that bind their ligands rapidly and reversibly.

### Cytoplasmic loop structure

In all GPCRs, CL2 and CL3 are believed to have an important role in the binding, selectivity and activation of G proteins, CL2 being

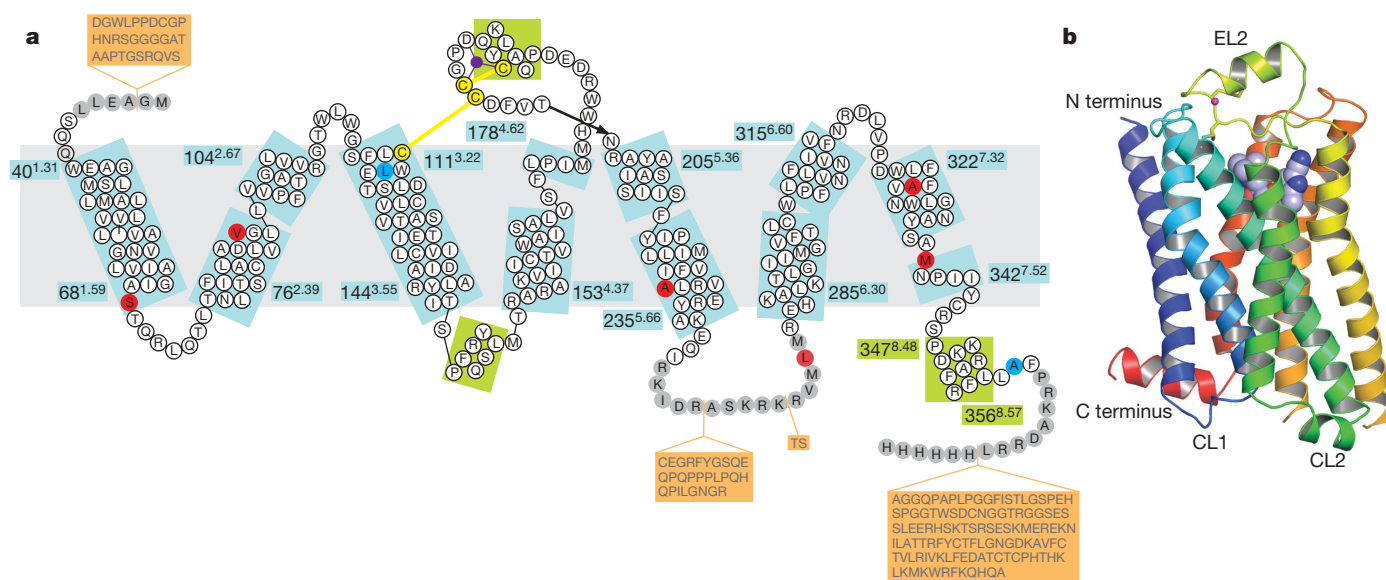


**Figure 1 | Schematic representations of the turkey  $\beta_1$ AR structure.**

**a**, Diagram of the turkey  $\beta_1$ AR sequence in relation to secondary structure elements. The residues in white circles indicate regions that are well ordered; the sequences in grey circles were not resolved in the structure. The sequences on an orange background were deleted to make the  $\beta_1$ AR construct for expression. Thermostabilizing mutations are in red circles and two other mutations—C116L (increases functional expression) and C358A (eliminates palmitoylation site)—are in blue circles. The Na<sup>+</sup> ion is in purple. Numbers refer to the first and last amino acid residues in each helix

(blue boxes), with the Ballesteros–Weinstein numbering in superscript. Helices were defined using the Kabsch and Sander algorithm<sup>49</sup>, with helix distortions being defined as residues that have main chain torsion angles that differ by more than 40° from standard  $\alpha$ -helix values (−60°, −40°). **b**, Ribbon representation of the  $\beta_1$ AR structure in rainbow colouration (N terminus, blue; C terminus, red), with the Na<sup>+</sup> ion in pink, the two near-by disulphide bonds in yellow, and cyanopindolol as a space-filling model. The extracellular loop 2 (EL2) and cytoplasmic loops 1 and 2 (CL1, CL2) are labelled.

important for the strength of the interaction and CL3 for specificity<sup>21–25</sup>. The  $\beta_1$ AR and  $\beta_2$ AR structures, along with rhodopsin<sup>26</sup>, have similar conformations for CL1, but there are major differences in CL2 and CL3. The CL3 differences are not of physiological relevance because they arise from deletions ( $\beta_1$ AR), deletion and insertion of T4 lysozyme ( $\beta_2$ AR–T4) or formation of an antibody complex ( $\beta_2$ AR–Fab), with only the rhodopsin structure having a native CL3 (ref. 26). However, differences in the conformation of CL2 (Fig. 2) are important, because this region is very highly conserved between  $\beta_1$ AR and  $\beta_2$ AR, although poorly conserved with rhodopsin. In  $\beta_1$ AR, CL2 forms a short  $\alpha$ -helix (residues Pro 146<sup>3,57</sup>–Leu 152<sup>3,63</sup>; Supplementary Fig. 9) parallel to the membrane surface whereas in both  $\beta_2$ AR structures and in rhodopsin this loop is in an extended conformation (Fig. 2). The  $\alpha$ -helical conformation of CL2 observed in  $\beta_1$ AR cannot be accommodated in either the  $\beta_2$ AR–Fab complex<sup>9</sup> or the  $\beta_2$ AR–T4 fusion<sup>10</sup> crystal structures because of lattice contacts with adjacent molecules. In  $\beta_1$ AR, CL2 also makes lattice contacts, but these are different between each of the four molecules and it is therefore likely that the helical conformation found here represents the physiologically relevant structure for all  $\beta$ ARs in the inactive conformation.

The CL2 loop has been proposed to function as the switch enabling G-protein activation<sup>21</sup>, and it is clear from the  $\beta_1$ AR structure that this short  $\alpha$ -helix interacts directly with the highly conserved Asp 138<sup>3,49</sup>Arg 139<sup>3,50</sup>Tyr 140<sup>3,51</sup> (DRY) motif in H3. Tyr 149 in CL2 is located sufficiently close to Asp 138<sup>3,49</sup> to allow the formation of a hydrogen bond (Fig. 2) between the tyrosine hydroxyl and the aspartate side chain. Supporting evidence for this structural role of Tyr 149 comes from the observation that the Y149A mutation makes  $\beta_1$ AR less thermally stable (Supplementary Table 2). The equivalent Tyr 141 in both  $\beta_2$ AR structures is in a cavity between H3, H4 and H6, but the biological relevance of this is unclear, owing to the perturbations in this region caused by either the T4 lysozyme fusion or by the bound antibody. Interestingly, a pattern of mutations consistent with an  $\alpha$ -helical conformation for CL2 was found in the muscarinic M5 receptor, and the equivalent M5 mutation Y138A led to increased

constitutive activity<sup>21</sup>. Thus, it is likely that both the tyrosine residue and the CL2  $\alpha$ -helix have key roles in G-protein coupling.

A salt bridge between Arg<sup>3,50</sup> and Glu<sup>6,30</sup>, termed the ‘ionic lock’ (Fig. 2), was proposed to have an essential role in maintaining GPCRs in an inactive state<sup>27</sup> but to break on receptor activation. Because the  $\beta_1$ AR structure represents a receptor lacking basal activity and containing bound antagonist, it is highly likely to represent the *R* conformation. However, this salt bridge is not present in either the  $\beta_1$ AR or the  $\beta_2$ AR structures (Fig. 2). This suggests that the ionic lock is not an essential feature of the inactive state. Even in dark-state rhodopsin, where these two charged residues are within hydrogen bonding distance<sup>26,28,29</sup>, the side chain B-factors of the two residues differ greatly (by 20–40 Å<sup>2</sup>)<sup>26</sup> so there is no direct experimental evidence for any ‘lock’.

### Selectivity of the ligand-binding pocket

The two  $\beta$ -receptor antagonists, cyanopindolol and carazolol, have very similar chemical structures (Supplementary Fig. 2) and both ligands bind with very high affinity to all  $\beta$ ARs. Carazolol is present in the ligand-binding pocket of both  $\beta_2$  structures, whereas the structure of  $\beta_1$  contains cyanopindolol. In the  $\beta_1$ AR structure there are 15 amino acid residues (using a 3.9 Å distance criterion) for which the side chains make contacts with cyanopindolol: 4 side chains are from H3, 3 are from H5, 4 are from H6, 2 are from H7 and 2 are from EL2 (Fig. 3). All of these residues are identical to those in human  $\beta_2$ AR, and the mode of binding of cyanopindolol to  $\beta_1$ AR is, therefore, similar to that of carazolol in  $\beta_2$ AR. However, the extra ring in the carazolol heterocyclic ring, owing to van der Waals contact with Tyr 199<sup>5,38</sup> in  $\beta_2$ AR, pushes the ligand more deeply into the binding site. The nitrogen in the cyano-moiety of cyanopindolol makes a weak hydrogen bond with the hydroxyl of Thr 203<sup>5,34</sup>, which is located together with Phe 201<sup>5,32</sup> on EL2 (Fig. 3). The same hydrogen bonds between the ligand and Asp 121<sup>3,32</sup>, Asn 329<sup>7,39</sup> and Ser 211<sup>5,42</sup> are present in both  $\beta_1$ AR and  $\beta_2$ AR structures, but the side-chain rotamer conformation of Ser 211<sup>5,42</sup> is different (Fig. 4 and Methods).

To explain why some ligands preferentially bind to either  $\beta_1$ AR or  $\beta_2$ AR, which is important in understanding the sub-type specificity of the human receptors<sup>11</sup>, there must be differences in amino acid residues close to the ligand-binding pocket that directly or indirectly affect binding. A comparison of residues within 8 Å of the binding pocket identified only two residues that are different between human  $\beta_1$ AR and  $\beta_2$ AR subtypes. The respective residues are Val 172<sup>4,56</sup> and Phe 325<sup>7,35</sup> in  $\beta_1$ AR, equivalent to Thr 164<sup>4,56</sup> and Tyr 308<sup>7,35</sup> in  $\beta_2$ AR. These differences introduce polar residues near the binding pocket of  $\beta_2$ AR relative to  $\beta_1$ AR (Fig. 4), which could affect ligand selectivity. Mutagenesis studies<sup>30,31</sup> have also implied that Tyr 308<sup>7,35</sup> is important for agonist selectivity in  $\beta_2$ AR. In  $\beta_2$ AR, Tyr 308<sup>7,35</sup> is positioned close to the binding pocket and can form a hydrogen bond to Asn 293<sup>6,55</sup>. In  $\beta_1$ AR the side chain of Asn 310<sup>6,55</sup> is closer to the cyano group of cyanopindolol and the equivalent residue, Phe 325<sup>7,35</sup>, is further from the binding pocket (Fig. 4). As a result, there is no contact between Phe 325<sup>7,35</sup> in  $\beta_1$ AR and cyanopindolol.

Part of the ligand-binding site is formed by EL2, and the backbone positions within this highly structured region of  $\beta_1$ AR differ from  $\beta_2$ AR by an r.m.s.d. of only 0.84 Å, compared with 0.63 Å between the same residues in molecules A and B in the unit cell. There are also significant differences in the primary amino acid sequence in this region that change the shape and charge distribution around the entrance to the ligand-binding pocket (Supplementary Fig. 10), with an ion pair formed between Asp 192<sup>5,31</sup> and Lys 305<sup>7,52</sup> in  $\beta_2$ AR that is absent in  $\beta_1$ AR because the respective residues are both aspartate (Asp 200<sup>5,31</sup> and Asp 322<sup>7,32</sup>). Differences between  $\beta_1$ AR and  $\beta_2$ AR in this region could affect ligand binding, especially for larger ligands with extensions that have direct interactions with non-conserved side chains. Recent mutational studies show that EL2 influences the specificity of ligand binding to both the normal (orthosteric) site<sup>32,33</sup> and

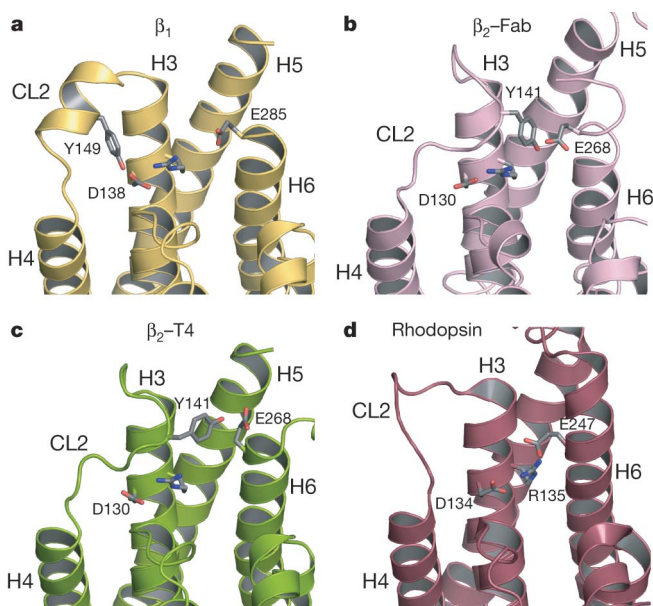


**Figure 2 | Comparison of the CL2 loop regions in four GPCR structures.** **a–d**, Shown are  $\beta_1$ AR (**a**), the  $\beta_2$ AR–Fab complex (**b**), the  $\beta_2$ AR–T4 lysozyme fusion (**c**) and rhodopsin (**d**). Residues DR from the highly conserved D<sup>3,48</sup>R<sup>3,49</sup>Y<sup>3,50</sup> motif are shown. Residue E<sup>6,30</sup>, which is half of the putative ionic lock, is also shown as E247 in rhodopsin, and E285 and E268 in  $\beta_2$ AR, respectively: E247<sup>6,30</sup> was thought to form a salt bridge with R135<sup>3,49</sup> in rhodopsin, but the evidence is weak. Finally, Y149 in  $\beta_1$  forms a hydrogen bond with D138<sup>3,48</sup> in  $\beta_1$ AR.

the sites of allosteric modulators<sup>34</sup>, and that the loop flexibility is important to the binding kinetics<sup>35</sup>.

The structure of  $\beta_1$ AR, when compared to that of  $\beta_2$ AR, provides a sound basis for studying selectivity differences between  $\beta$ AR antagonists that are structurally similar to cyanopindolol and carazolol. However, many ligands, such as the inverse agonist CGP 20712A (Supplementary Fig. 2), show very high selectivities<sup>11</sup> but are physically larger and structurally distinct from either cyanopindolol or carazolol. These ligands could well make contact with residues other than those described here.

### Agonist binding and GPCR activation

The  $\beta_1$ AR crystal structure shows the inactive state of the receptor, but it is notable that many agonists, including the natural ligands adrenaline and noradrenaline, are smaller than many of the best

antagonists, including cyanopindolol. Agonists have a shorter distance, by two carbon-carbon bonds or 2–3 Å, between the catechol hydroxyl groups or their equivalent and the obligatory amine nitrogen. We superimposed (Fig. 4b) a model of adrenaline with that of cyanopindolol and examined its relationship to the side chains of Asp 121<sup>3,32</sup> and Asn 329<sup>7,39</sup>, which make hydrogen bonds with the amine, and those of Ser 211<sup>5,42</sup>, Ser 212<sup>5,43</sup> and Ser 215<sup>5,46</sup>, which are expected to hydrogen bond with the meta- and para-hydroxyl groups on the catechol ring<sup>36–38</sup>. As noticed previously<sup>39</sup>, the catechol hydroxyl groups are well spaced and well oriented to interact with the side chain hydroxyl groups of Ser 211<sup>5,42</sup>, Ser 212<sup>5,43</sup> and Ser 215<sup>5,46</sup> on H5, but cannot reach far enough to make good hydrogen bonds if the amine occupies the same position as it does adjacent to Asp 121<sup>3,32</sup> in the cyanopindolol complex, without a substantial structural change in the receptor. It seems very reasonable that the

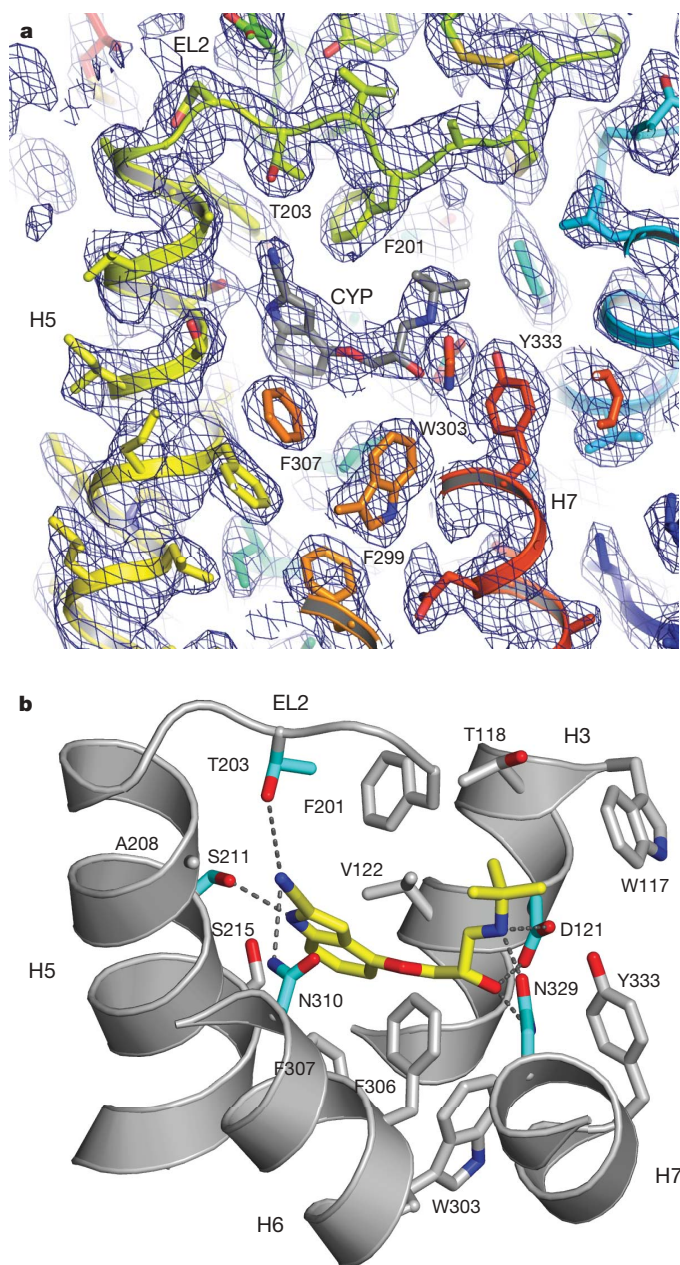


**Figure 3 | Structure of the ligand-binding pocket.** **a**,  $2F_o - F_c$  map before inclusion of cyanopindolol (CYP) in the model, showing the interaction of CYP with Thr 203 and Phe 201 in EL2. **b**, Amino acid residues that interact with the ligand cyanopindolol (yellow) by polar interactions (aquamarine) or non-polar interactions (grey).

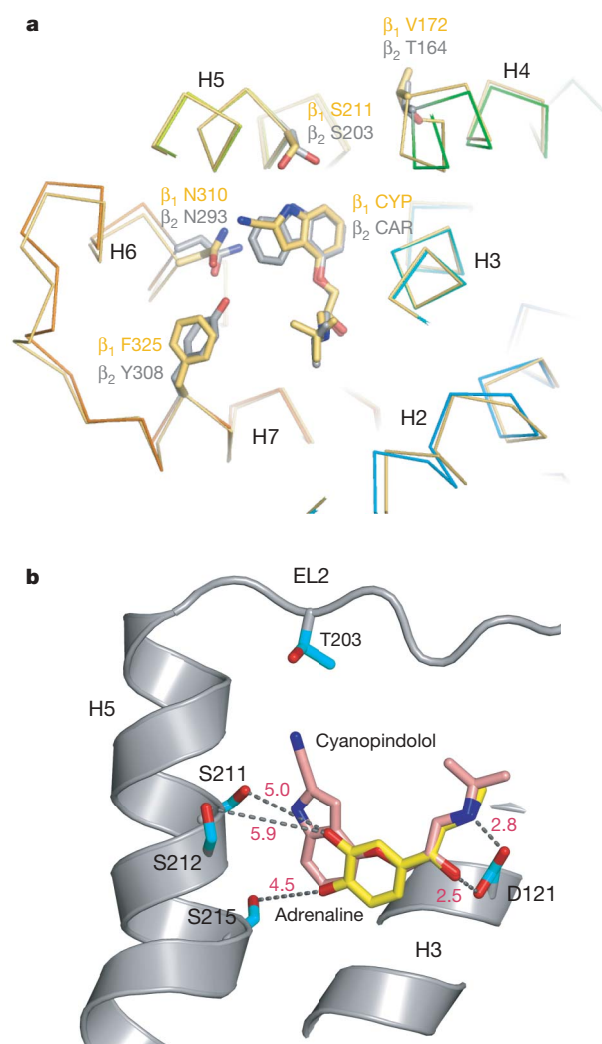


**Figure 4 | Comparisons between  $\beta$  receptor ligand-binding pockets and the binding of different ligands.** **a**, Superposition of  $\beta_1$ AR molecule B with  $\beta_2$ AR (PDB code 2RH1, ref. 10) in the region surrounding the ligand-binding site. Shown are side chains that have different rotamer conformations (N310<sup>6,55</sup> and S211<sup>5,42</sup>) along with two residues that are conserved yet consistently different between  $\beta_1$  and  $\beta_2$  receptors (F325/Y308<sup>7,35</sup> and V172/T164<sup>4,56</sup>). Cyanopindolol (CYP) is in the ligand-binding pocket of the  $\beta_1$  receptor, and carazolol (CAR) is in the  $\beta_2$  receptor. The biggest backbone deviation is seen at the V172/T164<sup>4,56</sup> position. **b**, Superposition of a model of the agonist, adrenaline (yellow), with the structure of the antagonist, cyanopindolol (pink), as it binds to  $\beta_1$ AR, showing the distances (in Å, red) to the nearest side chains known to interact with the hydroxyl groups on the catechol ring of the agonist. It is clear that a 2–3 Å tightening of the pocket around the ligand must occur on agonist binding.

ligand-binding site in  $\beta_1$ AR will contract by 2–3 Å on activation so that both ends of adrenaline can make good interactions with the residues on H3/H7 and H5. This view is also supported by engineered zinc-binding sites that activate the receptor<sup>40,41</sup>. How this tightening around the ligand-binding site could propagate to the cytoplasmic surface and cause an outward 5–6 Å movement of H6 (refs 2, 3) is difficult to predict, because all the transmembrane helices except H1 and H3 have pronounced kinks at conserved proline residues, which means they could easily bend. However, one speculation is that the pulling of H5 towards the centre of the receptor on activation could force H3 and H6 apart, causing cytoplasmic loops CL2 and CL3 to move apart, as observed in photoactivated rhodopsin<sup>3</sup>, and trigger recruitment of the G-protein complex.

## METHODS SUMMARY

**Purification and crystallization.** The  $\beta_1$ AR construct T34–424/His 6 (see ref. 42) was the starting point for the generation of the  $\beta_1$ AR36-m23 construct that crystallized. The C terminus was further truncated after Leu 367, and six histidines were added. Two segments, comprising residues 244–271 and 277–278 of CL3, were also deleted. The construct included the following eight point mutations: C116<sup>3,27</sup>L increased expression; C358A at the C terminus of H8 removed palmitoylation and helped crystallization; and R68<sup>1,59</sup>S, M90<sup>2,53</sup>V, Y227<sup>5,58</sup>A, A282<sup>9,27</sup>L, F327<sup>7,37</sup>A and F338<sup>7,48</sup>M thermostabilized the receptor in the antagonist conformation<sup>15</sup>. The receptor was expressed using the baculovirus system and then purified<sup>42</sup> in decylmaltoside, with a detergent exchange to octylthioglucoside on the alprenolol sepharose column. Crystals were obtained by vapour diffusion at 18 °C with hanging drops after addition of an equal volume of reservoir solution (0.1 M *N*-(2-acetamido)iminodiacetic acid:NaOH, pH 6.9–7.3, and 29–32% PEG600) to purified receptor (6.0 mg ml<sup>-1</sup>).

**Data collection, structure solution and refinement.** Diffraction data were collected from many crystals on beamlines ID13 and ID23-2 at ESRF, Grenoble<sup>43,44</sup>; the data used for structure determination were collected at ID23-2 with a 10 µm beam using three positions on a single cryo-cooled crystal (100 K). Images were processed with MOSFLM and SCALA<sup>45</sup>. The structure was solved by molecular replacement with PHASER<sup>46</sup>, using the structure of human  $\beta_2$ AR<sup>10</sup> as an initial model. All four copies of the molecule in the triclinic unit cell were located (Supplementary Figs 4 and 5). The amino acid sequence was corrected, and the model refined with PHENIX<sup>47</sup> and rebuilt with O<sup>48</sup> (see Methods for further details). An overview of the B-factor distribution for  $\beta_1$ AR molecules A and B is shown in Supplementary Fig. 6. Figures were produced using Pymol (DeLano Scientific LLC).

**Full Methods** and any associated references are available in the online version of the paper at [www.nature.com/nature](http://www.nature.com/nature).

Received 26 March; accepted 19 May 2008.

Published online 25 June 2008.

- Fredriksson, R. & Schiöth, H. B. The repertoire of G-protein-coupled receptors in fully sequenced genomes. *Mol. Pharmacol.* **67**, 1414–1425 (2005).
- Hubbell, W. L., Altenbach, C., Hubbell, C. M. & Khorana, H. G. Rhodopsin structure, dynamics, and activation: a perspective from crystallography, site-directed spin labeling, sulfhydryl reactivity, and disulfide cross-linking. *Adv. Protein Chem.* **63**, 243–290 (2003).
- Altenbach, C. *et al.* High resolution distance mapping in rhodopsin reveals the pattern of helix movement due to activation. *Proc. Natl Acad. Sci. USA* **105**, 7439–7444 (2008).
- Foord, S. M. *et al.* International Union of Pharmacology. XLVI. G protein-coupled receptor list. *Pharmacol. Rev.* **57**, 279–288 (2005).
- Baldwin, J. M., Schertler, G. F. & Unger, V. M. An alpha-carbon template for the transmembrane helices in the rhodopsin family of G-protein-coupled receptors. *J. Mol. Biol.* **272**, 144–164 (1997).
- Bockaert, J. & Pin, J. P. Molecular tinkering of G protein-coupled receptors: an evolutionary success. *EMBO J.* **18**, 1723–1729 (1999).
- Ballesteros, J. A. & Weinstein, H. Integrated methods for the construction of three dimensional models and computational probing of structure function relations in G protein-coupled receptors. *Methods Neurosci.* **25**, 366–428 (1995).
- Black, J. W. Drugs from emasculated hormones — the principle of synaptic antagonism (Nobel lecture). *Angew. Chem. Int. Edn Engl.* **28**, 886–894 (1989).
- Rasmussen, S. G. *et al.* Crystal structure of the human  $\beta_2$  adrenergic G-protein-coupled receptor. *Nature* **450**, 383–387 (2007).
- Cherezov, V. *et al.* High-resolution crystal structure of an engineered human  $\beta_2$ -adrenergic G protein-coupled receptor. *Science* **318**, 1258–1265 (2007).
- Baker, J. G. The selectivity of  $\beta$ -adrenoceptor antagonists at the human  $\beta_1$ ,  $\beta_2$  and  $\beta_3$  adrenoceptors. *Br. J. Pharmacol.* **144**, 317–322 (2005).
- Sugimoto, Y. *et al.*  $\beta_1$ -selective agonist (-)-1-(3,4-dimethoxyphenethylamino)-3-(3,4-dihydroxy)-2-propanol [(-)-RO363] differentially interacts with key amino acids responsible for  $\beta_1$ -selective binding in resting and active states. *J. Pharmacol. Exp. Ther.* **301**, 51–58 (2002).
- Gether, U. *et al.* Structural instability of a constitutively active G protein-coupled receptor. Agonist-independent activation due to conformational flexibility. *J. Biol. Chem.* **272**, 2587–2590 (1997).
- Parker, E. M., Kameyama, K., Higashijima, T. & Ross, E. M. Reconstitutively active G protein-coupled receptors purified from baculovirus-infected insect cells. *J. Biol. Chem.* **266**, 519–527 (1991).
- Serrano-Vega, M. J., Magnani, F., Shibata, Y. & Tate, C. G. Conformational thermostabilization of the beta1-adrenergic receptor in a detergent-resistant form. *Proc. Natl Acad. Sci. USA* **105**, 877–882 (2008).
- Baker, J. G. Site of action of  $\beta$ -ligands at the human  $\beta_1$ -adrenoceptor. *J. Pharmacol. Exp. Ther.* **313**, 1163–1171 (2005).
- Lattion, A., Abuin, L., Nenniger-Tosato, M. & Cotecchia, S. Constitutively active mutants of the  $\beta_1$ -adrenergic receptor. *FEBS Lett.* **457**, 302–306 (1999).
- Samama, P. *et al.* Negative antagonists promote an inactive conformation of the  $\beta_2$ -adrenergic receptor. *Mol. Pharmacol.* **45**, 390–394 (1994).
- Yarden, Y. *et al.* The avian  $\beta$ -adrenergic receptor: primary structure and membrane topology. *Proc. Natl Acad. Sci. USA* **83**, 6795–6799 (1986).
- Harding, M. M. Metal-ligand geometry relevant to proteins and in proteins: sodium and potassium. *Acta Crystallogr. D* **58**, 872–874 (2002).
- Burstein, E. S., Spalding, T. A. & Brann, M. R. The second intracellular loop of the m5 muscarinic receptor is the switch which enables G-protein coupling. *J. Biol. Chem.* **273**, 24322–24327 (1998).
- Wong, S. K. F., Parker, E. M. & Ross, E. M. Chimeric muscarinic cholinergic  $\beta$ -adrenergic receptors that activate Gs in response to muscarinic agonists. *J. Biol. Chem.* **265**, 6219–6224 (1990).
- Wong, S. K. F. & Ross, E. M. Chimeric muscarinic cholinergic: $\beta$ -adrenergic receptors that are functionally promiscuous among G-proteins. *J. Biol. Chem.* **269**, 18968–18976 (1994).
- Wess, J., Bonner, T. I., Dorje, F. & Brann, M. R. Delineation of muscarinic receptor domains conferring selectivity of coupling to guanine nucleotide-binding proteins and 2nd messengers. *Mol. Pharmacol.* **38**, 517–523 (1990).
- Scarselli, M., Li, B., Kim, S. K. & Wess, J. Multiple residues in the second extracellular loop are critical for M3 muscarinic acetylcholine receptor activation. *J. Biol. Chem.* **282**, 7385–7396 (2007).
- Li, J. *et al.* Structure of bovine rhodopsin in a trigonal crystal form. *J. Mol. Biol.* **343**, 1409–1438 (2004).
- Ballesteros, J. A. *et al.* Activation of the  $\beta_2$ -adrenergic receptor involves disruption of an ionic lock between the cytoplasmic ends of transmembrane segments 3 and 6. *J. Biol. Chem.* **276**, 29171–29177 (2001).
- Palczewski, K. *et al.* Crystal structure of rhodopsin: a G protein-coupled receptor. *Science* **289**, 739–745 (2000).
- Okada, T. *et al.* The retinal conformation and its environment in rhodopsin in light of a new 2.2 angstrom crystal structure. *J. Mol. Biol.* **342**, 571–583 (2004).
- Kikkawa, H., Isogaya, M., Nagao, T. & Kurose, H. The role of the seventh transmembrane region in high affinity binding of a  $\beta_2$ -selective agonist TA-2005. *Mol. Pharmacol.* **53**, 128–134 (1998).
- Isogaya, M. *et al.* Identification of a key amino acid of the  $\beta_2$ -adrenergic receptor for high affinity binding of salmeterol. *Mol. Pharmacol.* **54**, 616–622 (1998).
- Shi, L. & Javitch, J. A. The second extracellular loop of the dopamine D2 receptor lines the binding-site crevice. *Proc. Natl Acad. Sci. USA* **101**, 440–445 (2004).
- Klco, J. M., Wiegand, C. B., Narzinski, K. & Baranski, T. J. Essential role for the second extracellular loop in C5a receptor activation. *Nature Struct. Mol. Biol.* **12**, 320–326 (2005).
- Voigtlander, U. *et al.* Allosteric site on muscarinic acetylcholine receptors: Identification of two amino acids in the muscarinic M-2 receptor that account entirely for the M-2/M-5 subtype selectivities of some structurally diverse allosteric ligands in *N*-methylscopolamine-occupied receptors. *Mol. Pharmacol.* **64**, 21–31 (2003).
- Avlani, V. A. *et al.* Critical role for the second extracellular loop in the binding of both orthosteric and allosteric G protein-coupled receptor ligands. *J. Biol. Chem.* **282**, 25677–25686 (2007).
- Sato, T., Kobayashi, H., Nagao, T. & Kurose, H. Ser(203) as well as Ser(204) and Ser(207) in fifth transmembrane domain of the human  $\beta_2$ -adrenoceptor contributes to agonist binding and receptor activation. *Br. J. Pharmacol.* **128**, 272–274 (1999).
- Strader, C. D. *et al.* Identification of 2 serine residues involved in agonist activation of the  $\beta$ -adrenergic-receptor. *J. Biol. Chem.* **264**, 13572–13578 (1989).
- Liapakis, G. *et al.* The forgotten serine — A critical role for Ser-203(5.42) in ligand binding to and activation of the  $\beta_2$ -adrenergic receptor. *J. Biol. Chem.* **275**, 37779–37788 (2000).
- Rosenbaum, D. M. *et al.* GPCR engineering yields high-resolution structural insights into  $\beta_2$ -adrenergic receptor function. *Science* **318**, 1266–1273 (2007).
- Elling, C. E., Thirstrup, K., Holst, B. & Schwartz, T. W. Conversion of agonist site to metal-ion chelator site in the  $\beta_2$ -adrenergic receptor. *Proc. Natl Acad. Sci. USA* **96**, 12322–12327 (1999).
- Schwartz, T. W. *et al.* Molecular mechanism of 7TM receptor activation — a global toggle switch model. *Annu. Rev. Pharmacol. Toxicol.* **46**, 481–519 (2006).

42. Warne, T., Chirinside, J. & Schertler, G. F. Expression and purification of truncated, non-glycosylated turkey beta-adrenergic receptors for crystallization. *Biochim. Biophys. Acta* **1610**, 133–140 (2003).
43. Riek, C., Burghammer, M. & Schertler, G. Protein crystallography microdiffraction. *Curr. Opin. Struct. Biol.* **15**, 556–562 (2005).
44. Standfuss, J. *et al.* Crystal structure of a thermally stable rhodopsin mutant. *J. Mol. Biol.* **372**, 1179–1188 (2007).
45. Evans, P. Scaling and assessment of data quality. *Acta Crystallogr. D* **62**, 72–82 (2006).
46. McCoy, A. J. *et al.* Phaser crystallographic software. *J. Appl. Cryst.* **40**, 658–674 (2007).
47. Adams, P. D. *et al.* PHENIX: building new software for automated crystallographic structure determination. *Acta Crystallogr. D* **58**, 1948–1954 (2002).
48. Jones, T. A., Zou, J. Y., Cowan, S. W. & Kjeldgaard, M. Improved methods for building protein models in electron-density maps and the location of errors in these models. *Acta Crystallogr. A* **47**, 110–119 (1991).
49. Kabsch, W. & Sander, G. Dictionary of protein secondary structure: pattern recognition of hydrogen-bonded and geometrical features. *Biopolymers* **22**, 2577–2637 (1983).

**Supplementary Information** is linked to the online version of the paper at [www.nature.com/nature](http://www.nature.com/nature).

**Acknowledgements** This work was supported by a joint grant from Pfizer Global Research and Development and from the MRCT Development Gap Fund to C.G.T. and R.H., in addition to core funding from the MRC. G.F.X.S. was financially supported by a Human Frontier Science Project (HFSP) programme grant (RG/

0052), a European Commission FP6 specific targeted research project (LSH-2003-1.1.0-1) and an ESRF long-term proposal. J.G.B. is funded by a Wellcome Trust Clinician Scientist Fellowship. We thank E. Ross for his support in the initial stages of the  $\beta_1$ AR project at the LMB and for his comments on the manuscript. In addition, we would also like to thank R. Grisshammer, E. Hulme, F. Marshall and M. Weir, as well as J. Li, M. Babu and other colleagues at LMB for their comments. We also thank beamline staff at the European Synchrotron Radiation Facility, particularly C. Riek and M. Burghammer at ID13 and D. Flot and S. McSweeney at ID 23-2. Finally, we thank D. Loakes for Supplementary Fig. 2.

**Author Contributions** T.W. devised and carried out receptor expression, purification, crystallization and cryo-cooling of the crystals. Receptor stabilization and baculovirus expression were performed by M.J.S.-V.; both authors were also involved in data collection and preliminary crystallographic analyses of the crystals. P.C.E. helped with the crystal cryo-cooling strategy and in diffraction data collection. J.G.B. performed the functional cAMP and reporter gene assays. R.M. was involved in data collection and processing. A.G.W.L. processed the final data, solved and refined the structure, and assisted with manuscript preparation. The overall project management and manuscript preparation were by R.H., C.G.T. and G.F.X.S.

**Author Information** Co-ordinates and structure factors have been submitted to the PDB database under accession code 2vt4. Reprints and permissions information is available at [www.nature.com/reprints](http://www.nature.com/reprints). The authors declare competing financial interests: details accompany the paper on [www.nature.com/nature](http://www.nature.com/nature). Correspondence and requests for materials should be addressed to C.G.T. ([cgt@mrc-lmb.cam.ac.uk](mailto:cgt@mrc-lmb.cam.ac.uk)) or G.F.X.S. ([gfx@mrc-lmb.cam.ac.uk](mailto:gfx@mrc-lmb.cam.ac.uk)).

## METHODS

**Purification and crystallization.** Baculovirus expression in High 5 cells, membrane preparation, solubilization, IMAC and alprenolol sepharose chromatography were all performed as described previously<sup>42</sup>, except that solubilization and IMAC were performed in buffers containing the detergent decylmaltoside and the detergent was exchanged on the alprenolol sepharose column to octylthioglucoside; purified receptor was eluted from the alprenolol sepharose with cyanopindolol (30  $\mu$ M). The buffer was exchanged to 10 mM Tris-HCl, pH 7.7, 50 mM NaCl, 0.1 mM EDTA, 0.35% octylthioglucoside and 0.5 mM cyanopindolol during concentration to give a final receptor concentration of 5.5–6.0 mg ml<sup>-1</sup>.

Using the thermally stabilized protein, a wide crystal screen was performed in four different detergents. A total of 58 mg of receptor was used to set up 17,800 crystallization trials in an MRC ultraviolet transparent crystallization plate and imaged with the MRC multiwavelength imaging system at 380 nm. Promising looking crystals were then imaged at 280 nm to exclude salt and detergent crystals. The receptor crystallization in octylthioglucoside was optimised by vapour diffusion at 18 °C with hanging drops after addition of an equal volume of reservoir solution (0.1 M ADA, pH 6.9–7.3, and 29–32% PEG 600). Crystals were mounted on Hampton CrystalCap HT loops and were cryo-cooled in liquid nitrogen. Cryoprotection of crystals was achieved by increasing the PEG 600 concentration in the drop to 55–70%.

**Data collection, structure solution and refinement.** The first diffraction patterns from microcrystals grown in the primary crystallization screens were tested with a 5  $\mu$ m beam on beamline ID13 (ref. 43) at the European Synchrotron Radiation Facility, Grenoble. The best crystallization conditions were refined to improve diffraction quality and the optimized crystals were then screened at ID23-2 with a 10  $\mu$ m focused beam; the micro-beams helped to deal with heterogeneous diffraction within a single crystal. Diffraction data were collected with a Mar 225 CCD detector on the microfocus beamline ID23-2 (wavelength, 0.8726 Å) using three positions on a single cryo-cooled crystal (100 K) with dimensions 240  $\times$  40  $\times$  10  $\mu$ m.

During the refinement of the model with PHENIX, tight non-crystallographic symmetry restraints ( $\sigma = 0.025$  Å) were applied to chains A and D and to chains B and C, with an accompanying reduction in  $R_{\text{free}}$ . Molecules A and D differ from molecules B and C by 0.46 Å r.m.s.d. on main-chain atoms excluding the N terminus of kinked H1. Molecules B and C have 0.18 Å r.m.s.d. for 272 residues. Molecules A and D have 0.22 Å r.m.s.d. for 272 residues. The cyanopindolol ligand, detergent, water molecules and sodium ions were added at a late stage of refinement. Non-crystallographic restraints were not applied to detergent and water molecules. The correct side-chain rotamer of Ser 211 was ambiguous with both *gauche*<sup>+</sup> and *trans* rotamers giving an equally good fit to the electron density after refinement. The *gauche*<sup>+</sup> conformation was chosen because the *trans* conformation resulted in a short contact of 2.8 Å between the  $\beta$ -carbon of Ser 211 and the carbonyl oxygen of residue 207. In addition, the *gauche*<sup>+</sup> conformation allows the serine hydroxyl to act as both a hydrogen bond donor and an acceptor, whereas it can only act as an acceptor in the *trans* conformation. An overview of the B-factor distribution for  $\beta_1$ AR molecules A and B is shown in

Supplementary Fig. 6, alongside rhodopsin (PDB code 1GZM) and  $\beta_2$ AR-T4 (PDB code 2RH1).

**G-protein-coupling assays and cAMP measurement.** Stable cell lines expressing the  $\beta$ AR-m23 mutation were made. A stable clonal CHO-K1 cell line expressing a *CRE-SPAP* reporter gene (six cAMP response elements (*CRE*) upstream of a secreted placental alkaline phosphatase (*SPAP*) gene) was transfected with plasmid pcDNA3 containing the  $\beta$ AR-m23 complementary DNA. The transfected cells were selected by neomycin resistance (1 mg ml<sup>-1</sup>; for the turkey receptor) and hygromycin resistance (200  $\mu$ g ml<sup>-1</sup>; for the *CRE-SPAP* reporter gene) for three weeks, and then single clones were isolated by dilution cloning to give clonal lines (CHO-m23-SPAP cells).

Whole-cell binding assays using <sup>3</sup>H-CGP12177 were performed and the  $K_i$  values of available agonists and antagonists were determined from competition curves (J.G.B., unpublished observation). The ability of  $\beta$ AR-m23 to couple to G proteins was assessed by using a *CRE-SPAP* reporter assay as described previously<sup>50</sup>. In brief, confluent cells in serum-free medium were incubated for 5 h with the agonist, or after pre-treatment with antagonist for 1 h. Cells were then incubated for a further hour in the absence of ligands and the level of secreted alkaline phosphates then determined by a colorimetric reaction using pNPP. To determine what conformation  $\beta$ AR-m23 has in the absence of ligand, the effect of a known inverse agonist ICI 118551 was tested on the CHO-m23-SPAP cells. Confluent cells were pre-labelled with <sup>3</sup>H-adenine in serum-free medium for 2 h, were removed and then the cells were incubated in 100  $\mu$ M isobutylmethylxanthine (IBMX, a non-specific phosphodiesterase inhibitor) and ICI 118551. After 5 h the reaction was terminated and <sup>3</sup>H-cAMP separated from other <sup>3</sup>H-nucleotides by sequential Dowex and alumina column chromatography, as described previously<sup>51</sup>. Under these conditions any inverse agonist effects of ICI 118551 would have been seen<sup>52</sup>. Data for all experiments were analysed by GraphPad Prism; all data are presented as mean  $\pm$  s.e.m. of triplicate determinations, where  $n$  is the number of separate experiments. Using the same assay, cyanopindolol appeared to be a very weak partial agonist.

All agonist ligands used were examined in the parent CHO-SPAP cells (that is, cells expressing the reporter but not  $\beta$ AR-m23); no effects were seen in response to any of the ligands over a 10<sup>7</sup> concentration range despite an increase in *CRE-SPAP* production in response to 3  $\mu$ M forskolin. This suggests that all the responses in CHO-m23-SPAP cells were indeed occurring by means of  $\beta$ AR-m23. **Figure production.** The alignment of receptors (Supplementary Fig. 1) was performed using ClustalW (MacVector), and Supplementary Figs 4–6 and 8–10 were made using PyMol (DeLano Scientific LLC).

- Baker, J. G., Hall, I. P. & Hill, S. J. Agonist actions of "beta-blockers" provide evidence for two agonist activation sites or conformations of the human  $\beta_1$ -adrenoceptor. *Mol. Pharmacol.* **63**, 1312–1321 (2003).
- Donaldson, J., Brown, A. M. & Hill, S. J. Influence of rolipram on the cyclic 3',5'-adenosine monophosphate response to histamine and adenosine in slices of guinea-pig cerebral cortex. *Biochem. Pharmacol.* **37**, 715–723 (1988).
- Baker, J. G., Hall, I. P. & Hill, S. J. Agonist and inverse agonist actions of beta-blockers at the human  $\beta_2$ -adrenoceptor provide evidence for agonist-directed signaling. *Mol. Pharmacol.* **64**, 1357–1369 (2003).